Vibration Performance of a Three-Phase Asynchronous Motor With Air-Gap Eccentricity

Shen Chen, Xiong Xin*, Zheng Shaoshuai,Xu Ganghui
School of Mechatronic Engineering and Automation
Shanghai University
Shanghai, China
E-mail: xxiong@shu.edu.cn

***Abstract*—In this paper, the vibration performances of a three-phase asynchronous motor with air-gap eccentricity were studied. The governing equations of the eccentric rotor-bearing system was established by considering the nonlinear bearing contact forces and the unbalanced magnetic pull (UMP) acting on the rotor. The UMP was calculated at the axial position of the supporting bearings, by integrating the total air gap distribution along the axial and circumferential direction. The air gap distribution can be deduced from the stator, rotor MMF harmonics and their related harmonics. By substituting the UMP into the governing equations, numerical responses of the rotor-bearing system under air-gap eccentricity can be simulated. Results show that the shaft orbits at both two ends of the shaft reside on their eccentric positions, i.e., the orbits of two shaft ends with symmetric angular eccentricity have the opposite phase direction. Besides, in the power spectrum of the simulated acceleration, the second harmonic component turns out to be notable compared with the fundamental frequency**

Keywords-Dynamic model; Air gap distribution; Unbalanced magnetic pull; Vibration characteristics

I. INTRODUCTION

As being the main driving and executing components of the industrial system, the squirrel cage asynchronous motor is of considerable importance to the safety operation and reduce the production loss. Faults detection of squirrel cage asynchronous motor can effectively reduce the failure rate and the maintenance costs. Among the commonly seen motor faults, air gap eccentricity is one the mostly seen abnormal status during operation. Thus, it is necessary to monitor the vibration signals and detect the corresponding characteristics of the eccentric fault. Motor air-gap eccentricity mostly turns out to be mixed eccentricity, which means that static and dynamic eccentricity simultaneously exists. Dynamic eccentricity means that the rotor shaft is not aligned with its rotating center, while the static eccentricity means that the rotor rotates on its own axis but being off-center from its stator bore. The first problem led by the air-gap eccentricity is the resulting UMP.UMP can be defined as a pure lateral force acting among the stator and rotor, and the air-gap flux density on both sides of the motor are variational during the rotation. It is caused by the concentration of air-gap flux in the non-uniform air gap. Some academicians [1]-[5] listed examples of UMP calculations in several types of induction motors. M. Kabir and M. Bradford [6, 7] conducted some early research works on the measurement of radial UMPs in the static air-gap eccentric motor. Li [8] described the axial variation pattern of the air-gap eccentricity in the paper and discussed its influences on vibration performances. However, the above research mainly focused on the study of static eccentric motors. Burakov and Arkkio [9,10] investigated the methods of UMP calculation under the eccentricity rotation status, which being named by 'whirling eccentricity'. The UMP interacts with the motor structure, and as the shaft usually being a flexible one, its critical speeds could generate further impact. Relevant finite element analysis based studies can be found in [11, 12]. In reference [13], the calculation of UMP was considered ,when static and dynamic eccentricity exists both, and some simulated results turns out to be accurate compared with the experimental ones.

As a summation, dynamic model of the rotor-bearing system in a three-phase asynchronous motor was established by taking the air-gap eccentricity into consideration. Maxwell stress method was applied to calculate the unbalanced magnetic pull (UMP) acting on two motor bearings. By analyzing and comparing the vibration performances of the rotor-bearing system under normal operation and three typical eccentric conditions, i.e., one parallel and two angular misalignment status, the characteristic behaviors and the related frequency components of the malfunction motor was deduced to detect the eccentric faults.

II. ROTOR-BEARING MODEL WITH AIR-GAP ECCENTRICITY

When the exact air gap value differs from the average air gap, a variable magnetic flux will be generated, which being called the air-gap eccentricity. The change of magnetic flux then produces the radial UMP acting on the rotor. Fig. 1(a) shows the rotor-bearing system without air-gap eccentricity, while Fig. 1(b) shows the eccentric case.

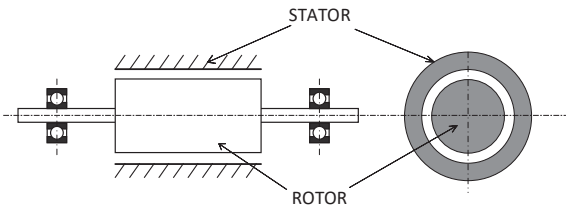

(a) Rotor system without air-gap eccentricity

978-1-7281-0860-5/19/$31.00 ©2019 IEEE

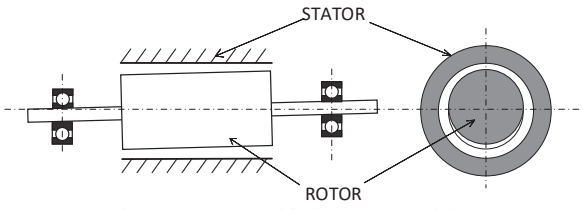

(b) Rotor system with air-gap eccentricity

Fig. 1 Schematic of the rotor-beairng system in induction motor

The outer ring of the supporting bearing is fixed through the bearing pedestal, and the inner ring rotates at the same speed of the shaft. When the rotor exhibits eccentricity, the entire rotor system is inclined, and the rotor system and its supporting bearing will be both affected by UMP and eccentric mass.

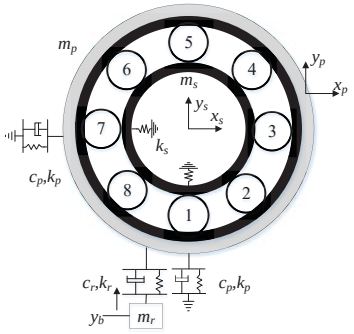

Fig. 2 Bearing coordinate system

The six-degree-of-freedom rotor-bearing model is shown in Fig. 2. For the bearing under radial load, the contact between the ball and the rings satisfies the nonlinear Hertz elastic contact theory, while the damping force is considered to be linear. $m_s, m_p, m_r, m_z$are respectively the mass of the bearing and inner-ring, outer ring together the bearing pedestal, the sprung mass and the eccentric mass in the disk. $k_p, k_s$and k_r are the stiffness of the bearing pedestal, the shaft and the sprung system. Two DOF $(x_m, y_m)$is describing the vibration responses of the mass disk. The inner-ring including the shaft and the outer-ring together with the bearing pedestal are defined by (x_s, y_s) and (x_p, y_p) respectively. The pedestal damping is defined by c_p and the damping of the sprung system is defined by c_r.

The cage evenly separates the n_b rollers (n_b=8), $j(j = 1,2\cdots, n_b)$ is the series number of the rolling element, $\phi_j$is the angular position of the j_{th} element, which is defined by

$$\phi_j = \frac{2\pi(j-1)}{n_b} + w_c t + \phi_0 \tag{1}$$

ϕ_0 is the initial position and w_c is the cage speed. δ_j defines the total deflection under contact load, while contact deflection between the inner-race and the outer-race.

$$\delta_j = (x_s - x_p)\cos\phi_j + (y_s - y_p)\sin\phi_j - a + R(\phi) \tag{2}$$

in which a represents the bearing clearance, and $R(\phi)$ represents the ring waviness. According to the Hertz contact theory, the relation of contact deformation and load between the ball and the raceway of outer and inner ring can be expressed as

$$Q = K\delta^n \tag{3}$$

in which, Q is the load, K is the contact stiffness, δ is the total deformation, n is the contact load deformation coefficient. In general, n=1.5 for the ball bearing. When the rolling bearing is under radial load, the sum of the elastic deformation can be decomposed into the deformation δ_o between the ball and the outer ring, and the deformation δ_i between the ball and the inner ring, which is

$$\delta = \delta_i + \delta_o \tag{4}$$

On the basis of the force balance condition, the force balance equation of each rolling body can be obtained as

$$K_i\delta_i^n - K_o\delta_o^n + F_{ej} = 0 \tag{5}$$

K_i, K_o represent the contact stiffness of the ball and the inner and outer ring. The centrifugal force of the spinning ball can be expressed as

$$F_{ej} = \frac{m_b d w_c^2}{2} \tag{6}$$

Using Newton-Raphson iterative algorithm, δ_i can be calculated according to the known quantity δ, then δ_o could further be obtained. Contact forces in the inner and outer ring can be deduced as

$$\begin{cases} F_{ix} = K_i \sum_{j=1}^{n_b} \gamma_j \delta_j^n \cos(\phi_j) \\ F_{iy} = K_i \sum_{j=1}^{n_b} \gamma_j \delta_j^n \sin(\phi_j) \\ F_{ox} = K_o \sum_{j=1}^{n_b} \gamma_j \delta_j^n \cos(\phi_j) \\ F_{oy} = K_o \sum_{j=1}^{n_b} \gamma_j \delta_j^n \sin(\phi_j) \end{cases} \tag{7}$$

F_{ix}, F_{iy} respectively represents the horizontal and vertical contact forces between the ball and the inner ring, while F_{ox}, F_{oy} respectively represent the horizontal and vertical contact forces between the ball and the outer ring. γ_j represents the contact status among the ball , the inner ring and outer ring (when $\delta_j > \delta_c$， $\gamma_j = 1$， otherwise$\gamma_j = 0$).

$$\delta_c = \left(\frac{m_b w_c^2 d}{2K_o}\right)^{1/n} \tag{8}$$

Taking the UMP and unbalanced force into consideration, the vibration equation of the rotor-bearing system with eccentric air-gap can be represented as fo.

$$\begin{cases} m_z\ddot{x}_m + k_s(x_m - x_s) = m_z r_z w_s^2 \cos(w_s t) \\ m_z\ddot{y}_m + k_s(y_m - y_s) = m_z r_z w_s^2 \sin(w_s t) \\ m_s\ddot{x}_s + k_s(x_s - x_m) = -F_{ix} - F_{UMP_x} \\ m_s\ddot{y}_s + k_s(y_s - y_m) = -F_{iy} - F_{UMP_y} \\ m_p\ddot{x}_p + c_p(\dot{x}_p - \dot{x}_b) + k_p(x_p - x_b) = F_{ox} \\ m_p\ddot{y}_p + c_p(\dot{y}_b - \dot{y}_b) + k_p(y_p - y_b) = F_{oy} \\ m_r\ddot{x}_b + c_r(\dot{x}_b - \dot{x}_p) + k_r(x_b - x_p) = 0 \\ m_r\ddot{y}_b + c_r(\dot{y}_b - \dot{y}_p) + k_r(y_b - y_p) = 0 \end{cases} \tag{9}$$

III. CALCULATION OF THE UNBALANCED MAGNETIC PULL

If the motor exits static eccentricity, series of air-gap magnetic density waves will be generated in the rotor system, that is, the magnetic density will pass through the air gaps in the radial direction of the stator and rotor surface and act on the Maxwell stress in the radial direction of the rotor surface, as shown in Fig. 3. The radial UMP is then calculated in a certain axial position.

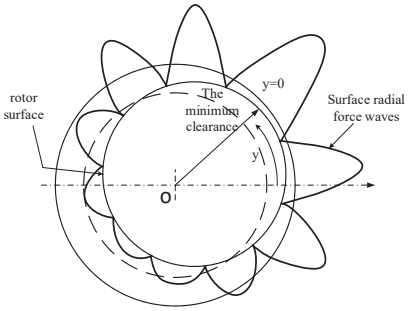

Fig. 3 Radial force waves on rotor surface caused by air-gap eccentricity

Stator magnetic density wave is one important source of UMP. The air-gap length g_s can be represented as equation (10), which is related to axial and circumferential coordinate *x* and *y*.

$$g_s(x,y) = g(1 - d_s(x)\cos(ky)) \tag{10}$$

$$ky = w_r t + ky' \tag{11}$$

$$k = 1/\mathrm{r} \tag{12}$$

$$w_r = (1 - s/p_m)w \tag{13}$$

$$g_s' = g\sqrt{1 - {D_s}^2} \tag{14}$$

in which, g is the average air gap length, and $d_s(x)$ is the eccentricity; y' is the position of a certain angle at a certain time instant for the rotor, w_r is the actual speed, and r is the mean radius of the air-gap; w is the input speed, s is the slip ratio. p_m is the main pole; D_s is the maximum unit deviation of the rotor. Air gap permeability can be obtained by inverting the length of air gap, as shown in the equation

$$\Lambda_s(x,y) = \frac{1}{g_s'}(1 + \sum 2\delta_s(x)\cos(ky)) \tag{15}$$

$\delta_s(x)$ is the maximum value of rotor offset, which is related to eccentricity types. When the eccentricity of the motor is not affected by the axial length, that is, when the motor is uniformly eccentric, then

$$\delta_s(x) = \Delta_s \tag{16}$$

When the eccentricity increases linearly along the axial direction, that is, only one end of the rotor is eccentric, then

$$\delta_s(x) = (L_{st} + 2x)\Delta_s/2L_{st} \tag{17}$$

If the eccentricity is same in size but in opposite directions at each side,then:

$$\delta_s(x) = (2x\Delta_s/L_{st}) \tag{18}$$

The air gap magnetic density of the stator is expressed as

$$b_{st}(y,t) = \Lambda_s(x,y)(\int \mu_0 j_{st}(y,t)\,dy + C_{Homopolar} \tag{19}$$

in which, $j_{st}(y,t)$ is the surface current density, $C_{\mathrm{Homopolar}}$ is the same magnetic flux integral constant, and the air gap magnetic density of the stator of the non-bipolar motor is expressed as

$$\begin{aligned} b_{st}(y,t) = Re \sum_{n=-\infty}^{\infty} [&\bar{B}_{st}^{np_m} e^{j(wt - np_m ky)} \\ &+ \bar{B}_{st}^{np_m-1}(x) e^{j(wt - k(np_m-1)y)} \\ &+ \bar{B}_{st}^{np_m+1}(x) e^{j(wt - k(p_m+1)y)}] \end{aligned} \tag{20}$$

$$\bar{B}_S^{np_m} = \frac{j\mu_0 \bar{J}_{st}^n}{knp_m g_s'} \tag{21}$$

$$\bar{B}_S^{np_m \pm 1}(x) = \frac{j\mu_0 \bar{J}_{st}^n}{knp_m g_s'}\delta_s(x) \tag{22}$$

μ_0 is the air permeability, $\bar{J}_{st}^n$ is the stator magnetomotive force amplitude.

In the calculation of UMP, most of the studies only consider the main magnetic density wave. In fact, rotor slip magnetic density wave cannot be neglected in UMP calculation. The magnetic density wave relationship between stator and rotor is shown in Table 1. For $p = np_m$, only stator magnetic density wave exists, while for $p = np_m$ and $p = np_m \pm 1$, rotor magnetic density wave exists.

Table I. STATOR AND ROTOR MMF WAVES ANDASSOCIATED AIR-GAP HARMONIC WAVES

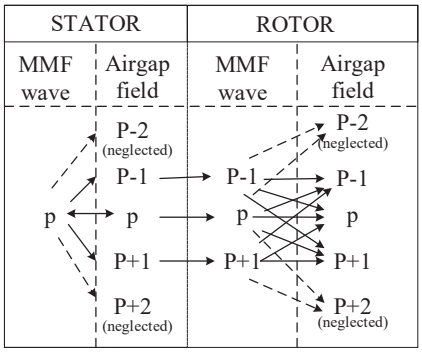

Similar to the calculation of stator's air-gap magnetic density, it is worth noting that rotor's air-gap magnetic density wave generally variates along the axial direction *x*, and the rotor's air-gap magnetic density can be obtained as

$$\begin{aligned} b_r(x,y,t) = Re \sum_{n=-\infty}^{\infty} [&\bar{B}_{r(p,p\pm1)}^{p}(x) e^{j(wt - np_m ky)} \\ &+ \bar{B}_{r(p,p\pm1)}^{np_m-1}(x) e^{j(wt - k(np_m-1)y)} \\ &+ \bar{B}_{r(p,p\pm1)}^{np_m+1}(x) e^{j(wt - k(p_m+1)y)}] \end{aligned} \tag{23}$$

$$\bar{B}_r^{np_m} = \frac{j\mu_0 N_b \bar{N}_r^p \bar{I}_r^p}{knp_m g_s'} \tag{24}$$

$$\bar{B}_r^{np_m \pm 1}(x) = \frac{j\mu_0 N_b \bar{N}_r^p \bar{I}_r^p}{knp_m g_s'}\delta_s(x) \tag{25}$$

N_b is the number of rotor bars; $\overline{N}_r^p$ is winding distribution; $\overline{I}_r^p$ is the rotor current. The air-gap magnetic density of the motor is obtained by the synthesis of rotor and stator air-gap magnetic density.

$$\left(b(x,y,t)\right)^2 = \left(b_s(y,t)\right)^2 + (b_r(x,y,t))^2 + 2b_s(y,t)b_r(x,y,t) \tag{26}$$

Then the Maxwell perpendicular stress to a point on the rotor surface is

$$\sigma = \frac{1}{2\mu_0}\,(b(x,y,t))^2 \tag{27}$$

The UMP acting on both bearings (Subscript 1 - the left-end bearing, Subscript 2 - the right-end bearing) with eccentric air gap in a certain direction is expressed as

$$F_{bearing1}(t) = \frac{1}{L_{st}} \int_{-\frac{L_{st}}{2}}^{-\frac{L_{st}}{2}} \int_{0}^{2\pi r} \frac{\left(b(x,y,t)\right)^2}{2\mu_0}\left(\frac{L_{st}}{2}+x\right) cos(ky)dydx$$

$$F_{bearing2}(t) = \frac{1}{L_{st}} \int_{-\frac{L_{st}}{2}}^{-\frac{L_{st}}{2}} \int_{0}^{2\pi r} \frac{\left(b(x,y,t)\right)^2}{2\mu_0}\left(\frac{L_{st}}{2}-x\right) cos(ky)dydx \tag{28}$$

IV. NUMERCIAL SIMULATIONS

Vibration performance of three-phase asynchronous motor with air-gap eccentricity fault are investigated by numerically solving the established governing equations of the rotor-bearing system using Runge-Kutta method. The structural parameters of the induction motor used in the simulation are as follows: the main pole of the motor p_m =1, frequency of rotation f_i=20, number of stator slots z_1=36, number of rotor slots z_2 =32, air gap radius *R*=82.5mm, and air gap length *L*=0.19mm.

A. Motor Air-Gap flux density

The variation of air gap magnetic density along the circumferential position for static eccentricity is shown in Fig.4.

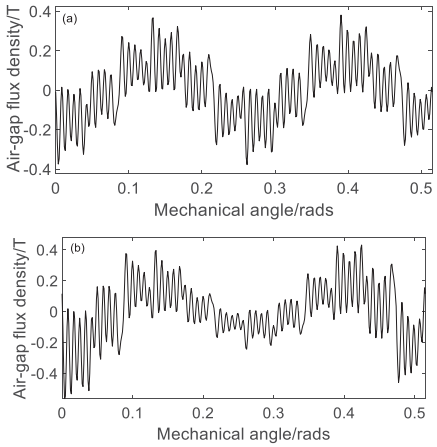

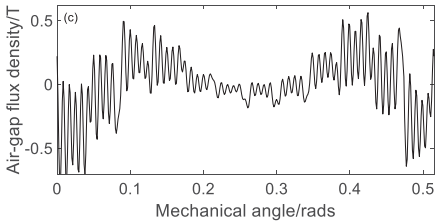

Fig. 4 Air gap flux density diagram,(a) $\varepsilon = 0$ (b) $\varepsilon = 0.2$ (c) $\varepsilon = 0.5$

If no air-gap eccentricity exists, the distribution of its magnetic field lines is symmetrical, and the magnetic density is uniform and periodical. For static eccentricity, the value of magnetic density in the area is concentrated and being amplified by the magnetic field lines, while the magnetic density value deviates from the small area of the air gap. Fig. 4(b)-(c) are respectively magnetic density diagrams for the conditions that the eccentricity is 0.2 and 0.5. By comparing the three magnetic density diagrams, it is concluded that the magnetic density of the narrow air gap increases with the increase of eccentricity, while the magnetic density of the large air gap decreases.

B. Dynamic behavior of the rotor-bearing system with air-gap eccentricity

The influence of UMP on the rotor system is analyzed for three cases. For the parallel eccentricity, the eccentricity is constant, that is, the eccentric rotating axis does not change along the axial direction. As for the unilateral eccentricity, eccentricity only occurs at one end of the rotor. The third case is the axisymmetric eccentricity, which means that eccentricity is in opposite direction at both ends but with equal size.

For parallel eccentricity, the UMPs acting on the bearings are identical at both ends of the rotor as shown in Fig. 5.

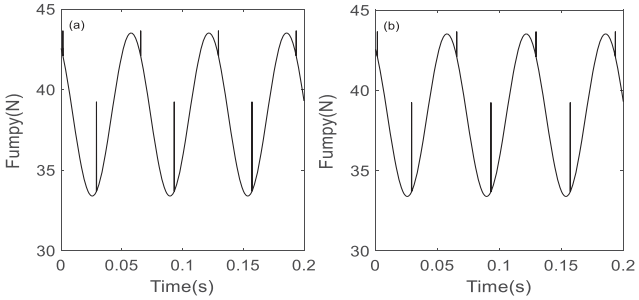

Fig. 5 UMP wavefom of (a) the left bearing and (b) the right bearing for parallel eccentricity

It can be seen that the greater the value of UMP, the stronger the impact exists in the harmonic waveform. The fault type can also be detected from the shaft orbit of the bearings at both ends, as shown in Fig. 5. Same orbits at both two ends means the parallel eccentricity exist in the rotor-bearing system of the induction motor. It can be seen that the vibration amplitude in the *y* direction is larger than the amplitude in the *x* direction.

As being shown in Fig. 7, the occurrence of air-gap eccentric results in a frequency constitution of the rotating

frequency 20 Hz and its second harmonic 40 Hz, which induced by the rotor eccentricity. Besides, the frequency constitution of the two spectrums are the same for both ends of the bearing, which indicated the parallel eccentricity fault.

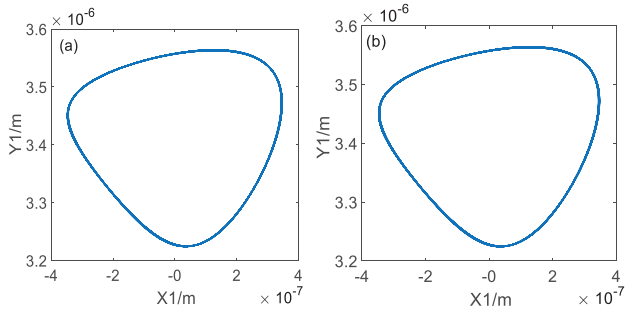

Fig. 6 The parallel eccentricity shaft orbit of (a) the left bearing and (b) the right bearin

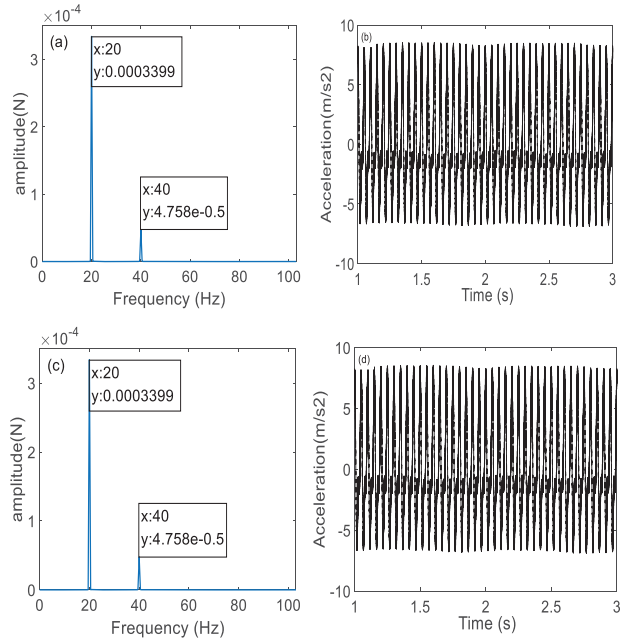

Fig. 7 Amplitude and its spectrum of the rotor at (a)-(b) the left bearing and (c)-(d) the right bearing for parallel eccentricity

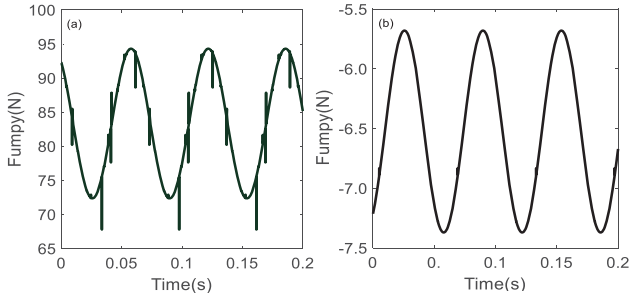

Fig. 8 UMP wavefom of (a) the left bearing and (b) the right bearing for unilateral eccentricity

For the simulation of the unilateral eccentricity, air-gap eccentricity is assigned at the left end of the rotor. The UMP waveforms at the left and right end bearings are obtained by numerical calculation.

It can be seen from Fig. 8 that UMP on the left bearing is larger than that on the right bearing. The impulsive effects of UMP on the left end bearing is strong, comparing with a harmonic counterpart at the right end bearing. Compared with the shaft orbit at both ends, the bearings at both ends deviated from the stator center, while in the *y* direction, deviation turns out to be notable compared with that of the *x* direction, as shown in Fig. 9. Besides, bearing positions at both ends are opposite, and the motion amplitudes in the *y* direction of the left end bearing is larger than that of the right end bearing. The UMP mainly acts on the left end of the rotor.

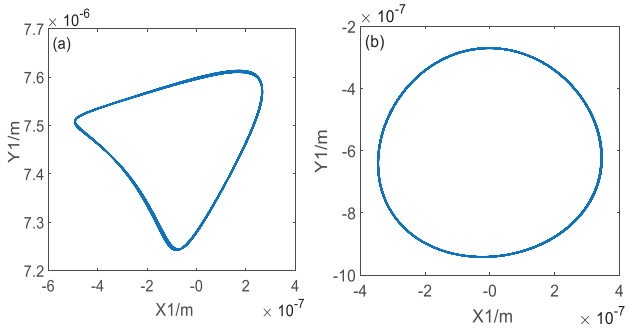

Fig. 9 The unilateral eccentricity shaft orbit of (a) the left bearing and (b) the right bearing

A comparison between the vibration spectrum of the left and right end bearing shows that the second harmonic of the rotating frequency due to the unilateral eccentricity is much stronger than that of the right end bearing.

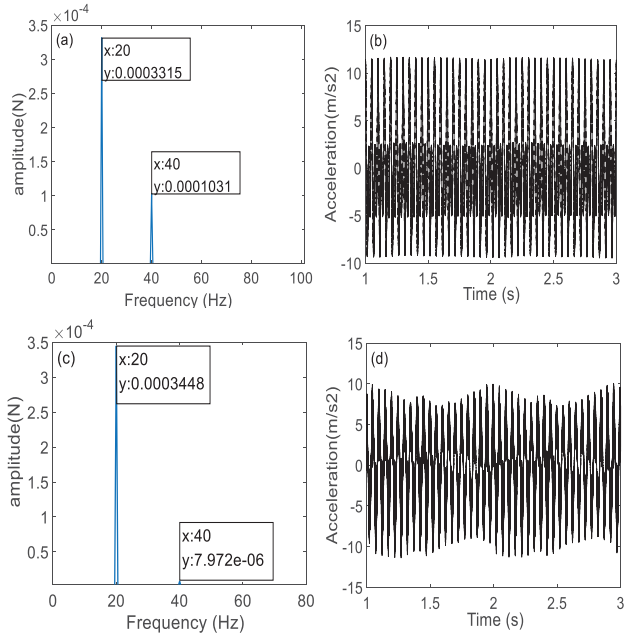

Fig. 10 Amplitude and its spectrum of the rotor at (a)-(b) the left bearing and (c)-(d) the right bearing for unilateral eccentricity

If the rotor is axially symmetric eccentric in the stator bore, the UMP waveform is shown in Fig. 11.

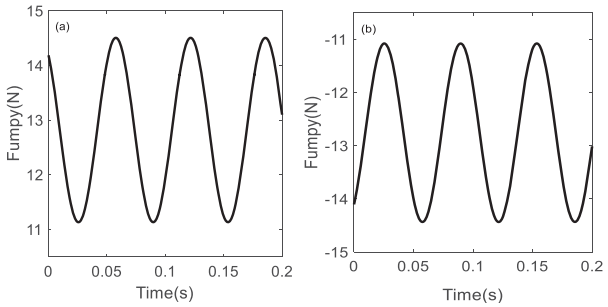

Fig. 11 UMP wavefom of (a) the left bearing and (b) the right bearing for symmetric eccentricity

UMP on the left bearing is equal to that on the right bearing, but with an opposite direction. It can also be seen from the shaft orbit of the two bearings in Fig. 12 that the shaft position is axially symmetric at both ends. Moreover, the orbit range is similar between the two ends. The vibration spectrum in Fig. 13 shows that the frequency constitution of the left bearing is similar to that of the right bearing, which means that the left and right bearing bear the same UMP load.

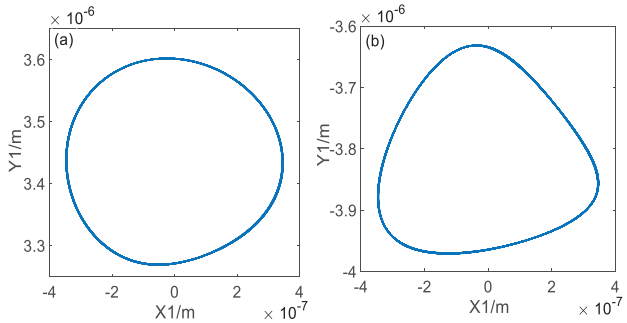

Fig.12 The symmetric eccentricity shaft orbit of (a) the left bearing and (b) the right bearing

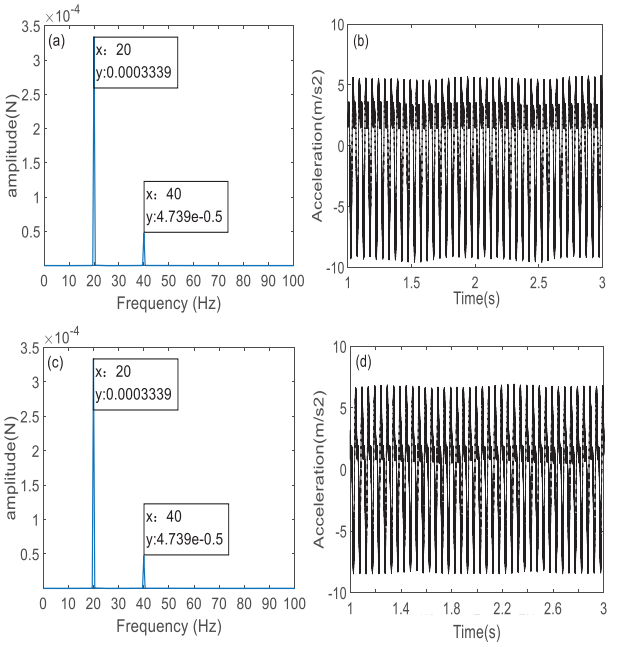

Fig .13 Amplitude and its spectrum of the rotor at (a)-(b) the left bearing and (c)-(d) the right bearing for symmetric eccentricity

V. Conclusions

This paper studied the vibration behavior of the three-phase asynchronous motor when air-gap eccentricity exists. According to the established 8 DOFs model, the numerically solved responses were analyzed according to the shaft orbit and the vibration displacement at both shaft ends. Besides, UMPs were calculated by considering the variation of magnetic field distribution according to the three eccentric cases.

(1) When static eccentricity exists, the magnetic field distribution concentrates in the narrow air gap space. The larger the eccentricity, the larger the magnetic density is in the narrow space and vice versa. The larger the eccentricity, the more significant the influence of UMP on rotor vibration. The increasement of air gap eccentricity results in a larger vibration amplitude and the impact effect.

(2) When air-gap eccentricity occurs, the second harmonic of the rotating frequency turns out to be notable compared with the rotating frequency, which can be applied as the indicator of air-gap eccentricity. Besides, the type of eccentricity can be further determined by comparing the shaft orbits at both ends of the rotor.

References

[1] Hawwooi C, Shek Jonathan K.H., “Calculation of unbalanced magnetic pull in induction machines through empirical method,”Iet Electric Power Applications, 2018, 12(9): 1233-1239.

[2] Di C , Bao X , Wang H , “Modeling and Analysis of Unbalanced Magnetic Pull in Cage Induction Motors With Curved Dynamic Eccentricity,” IEEE Trans. Magn, 2015, 51(8): 1-7.

[3] Pillai K P P , Nair A S , Bindu G R , “Unbalanced Magnetic Pull in Train-Lighting Brushless Alternators With Static Eccentricity,” IEEE Trans. on Vehicular Technology, 2008, 57(1):120-126.

[4] Michon,M., Holehouse, R.C., Atallah,K., “Effect of rotor eccentricity in large synchronous machines,”IEEE Trans. Magn, 2014, 50 (11):1–4

[5] Werner,U., “Rotor dynamic model for electromagnetic excitation caused by an eccentric and angular rotor core in ani nduction motor,”Arch. Appl. Mech. ,2013,83(8):1215–1238.

[6] Md Ashfanoor Kabir, and Adeeb Ahmed, “Axial flux segmental rotor flux-switching synchronous motor,” IEEE Trans. Magn, 2015,1: 330–338.

[7] M. Bradford, “Unbalanced magnetic pull in a 6-pole induction motor,” Proc. Inst. Elect. Eng, 2010,115: 1619–1627.

[8] X. Li, Q. Wu, and S. Nandi, “Performance analysis of a three-phase induction machine with inclined static eccentricity,” IEEE Trans. Ind. Appl, 2007,43(2): 531–541.

[9] A.Burakov and A.Arkkio, “Low-order parametric force model for eccentric rotor electrical machine equipped with parallel stator windings and rotor cage,” IET Elect. Power Appl, 2007,1(4): 532–542.

[10] Li, Y.,Hao, L.L.,Sun, Y.G., “The Analysis of UMP Caused by Non-salient Pole Synchronous Generator Rotor Winding Inter-turn Short Circuit Fault,”Autom. Electr. Power Syst, 2016, 40:81–89.

[11] A. C. Smith and D. G. Dorrell, “The detection and suppression of unbalanced magnetic pull in wound rotor induction motors using pole-specific search coils and auxiliary windings,” IEEE Trans.Magn, 2017, 53: 2066–2076.

[12] M. J. DeBortoli, S. J. Salon, D. W. Burow, and C. J. Slavik, “Effects of rotor eccentricity and parallel windings on induction machine behaviour: A study using finite element analysis.,” IEEE Trans. Magn, 2002,29(2): 1676–1682.

[13] D. G. Dorrell and O. Kayani, “Measurement and calculation of unbalanced magnetic pull in wound rotor induction machine,” IEEE Trans. Magn., 2014, 50(11):193-201.